Catalysis Today 413-415 (2023) 113994

Contents lists available at ScienceDirect

Catalysis Today

journal homepage: www.elsevier.com/locate/cattod

Photoreactivity of new rose bengal-SiO_2 heterogeneous photocatalysts with and without a magnetite core for drug degradation and disinfection

Jenny Flores [a], Pilar Moya [b], Francisco Bosca [a,*], M. Luisa Marin [a,*]

[a] Instituto de Tecnología Química, Universitat Politècnica de València-Consejo Superior de Investigaciones Científicas, Avda. de los Naranjos s/n, E-46022 Valencia, Spain

[b] Centro de Ecología Química Agrícola, Instituto Agroforestal Mediterráneo, Universitat Politècnica de València, Valencia, Spain

ARTICLE INFO

Keywords:
Electron transfer
Core@Shell NPs
Photodegradation mechanism
Photophysical data
Singlet oxygen

ABSTRACT

The main drawback of homogeneous photocatalysis is the difficult separation of the photocatalysts from the reaction media after treatment completion; thus, heterogeneous photocatalysis represents a step forward in this technology. Moreover, heterogeneous catalysts incorporating magnetic properties further facilitate their separation and recovery. In this context, some photocatalyst of Rose Bengal (RB) on heterogeneous supports have been synthesized but how derivatization influences its mechanism of action against organic pollutants degradation and water disinfection still deserves a deeper investigation. In this context, new heterogeneous nanosized photocatalysts incorporating Rose Bengal (RB) have been prepared. The first one was based on the covalent anchoring to SiO_2 nanoparticles and the second one incorporates a magnetite core. They have demonstrated to efficiently achieve photodegradation of ACF, DCF, and OFX under visible-light irradiation, with greater efficiency in the case of DCF. Interestingly, the photostability of RB is higher in heterogeneous than in homogeneous media. The presence of magnetite core in the heterogeneous photocatalyst facilitates its recovery from the medium but the photophysical properties of RB remain unchanged. These new photocatalysts also show a great efficiency in the photoinactivation of *Enterococcus faecalis* Gram-positive bacteria but not for the Gram-negative *Escherichia coli* and *Pseudomonas aeruginosa*. Analysis of all constants involving the photosensitized degradations of ACF, DCF, and OFX has evidenced that electron transfer process between RB, in homogeneous solutions and as a heterogeneous photocatalyst, and the three drugs is the initial step of their oxidations. In view of the results achieved, we believe that they could be used as a starting point for the development of new RB heterogeneous photocatalyst with adjustable oxidizing properties.

1. Introduction

The continuous growth of population and industrialization results in the presence of a large number of pollutants in aquatic bodies that are poorly abated through conventional wastewater treatment plants [1]. In fact, more than 4000 active substances are available on the market, and many of them and/or their metabolites have been found in natural and municipal wastewater [2,3]. Among them, pain relievers, non-steroidal anti-inflammatory drugs (NSAIDs), and antibiotics, including fluoroquinolones (FQs), are among the most widely used pharmaceuticals worldwide [4–6]. Many of the compounds that have been detected in effluents of European sewage treatment plant (STP), such as paracetamol (10–23.33 μg/L), diclofenac (0.01–510 μg/L), and ofloxacin (0.89–31.7 μg/L) are fully synthetic and are classified as emerging pollutants [2,7]. Moreover, the problem of the occurrence of microorganisms in water sources in developed countries is associated to cross-contamination of public access waters [8].

Advanced oxidation processes (AOPs) based on the absorption of light are characterized by the generation of highly reactive oxygen species (ROS), such as hydroxyl radical or singlet oxygen [9]. The photocatalysts employed for such purposes are mainly based on semiconductors, being TiO_2 the most representative example [10]. Photocatalysis constitutes an already mature technology that has been applied to degrade recalcitrant pollutants and to produce inactivation of bacteria [11,12]. More recently, newer materials like visible-light absorbing polymeric graphitic carbon nitrides [13], Ag_3VO_4 decorated phosphorus and sulphur co-doped graphitic carbon nitride [14], BiOI/Fe_3O_4 @graphene oxide ternary photocatalyst [15], or carbon quantum dots

* Corresponding authors.
E-mail addresses: fbosca@itq.upv.es (F. Bosca), marmarin@qim.upv.es (M.L. Marin).

https://doi.org/10.1016/j.cattod.2023.01.001
Received 31 August 2022; Received in revised form 28 December 2022; Accepted 2 January 2023
Available online 4 January 2023

supported AgI /ZnO/phosphorus doped graphitic carbon nitride [16], among others, have been reported as hybrid heterogeneous photocatalysts with good efficiency in decontamination and/or disinfection.

Furthermore, photocatalysis based on visible-light absorbing organic dyes is receiving increasing attention, as it offers great potential for the removal of organic pollutants, it is environmentally friendly and sustainable, and allows evaluating the kinetics of the starting steps of decontamination/disinfection, thus shedding light into the operating mechanisms [17,18]. Moreover, water disinfection by photodynamic inactivation of microorganisms offers great advantages over conventional water remediation processes, avoiding microbial resistance [19].

In this context, Rose Bengal (RB) is a non-toxic and metal-free organic dye with a strong absorption band in the green region of the visible spectrum (λ_{max} = 550 nm), a long-lived triplet excited state (0.1–0.3 ms) and a high singlet oxygen quantum yield ($\Phi_{\Delta} = 0.76$), that has been widely applied as a photocatalyst in decontamination/disinfection of wastewaters [20,21]. Recently, RB has proven to produce the oxidation of pollutants through photoinduced electron transfer mainly from its triplet excited state, upon absorption of visible light. It also generates singlet oxygen, a key ROS mainly responsible for the inactivation of bacteria [20–22].

However, the main drawback of homogeneous photocatalysis is the difficult separation of the photocatalysts from the reaction media after treatment completion; thus, heterogeneous photocatalysis represents a step forward in this technology when it is based on organic dyes [23]. Moreover, heterogeneous catalysts incorporating magnetic properties further facilitate their separation and recovery [24,25].

Furthermore, we have recently demonstrated that heterogenization of an organic dye on an inorganic support has a strong influence in its behaviour. For instance, we have synthesized a new photocatalyst based on riboflavin (SiO_2-RF) with enhanced stability due to a shell completely filled with RF that produces quick deactivation of ^{1}RF*, preventing formation of ^{3}RF* and $^1O_2$. The high adsorption of organic pollutants to the surface results in electron transfer to the short-lived ^{1}RF* producing oxidation through Type I mechanism [26]. This constitutes an example of how heterogenization results in different mechanisms of action that cannot be anticipated from the homogeneous behaviour, but have to be investigated.

In this regard, RB has been incorporated in different systems that include organic and inorganic nano-carriers to improve biopharmaceutical profile and enhance **RB**-based therapy [27]. Moreover, **RB** has been embedded within the pores and/or external surface of mesoporous silica materials to prevent aggregation and ensure production of $^1O_2$ for photodynamic therapy [28,29]. Furthermore, silica nanoparticles derivatized with **RB** have proven to efficiently inactivate Gram-positive bacteria [30]. In a recent paper **RB** has been covalently attached to the surface of silica in a hybrid structure (**RB**-decorated silica-coated silver nanocubes). The plasmonic effect of Ag nanoparticles on **RB** results in enhanced $^1O_2$ production [31]. This piece of work is a good example of a different behaviour based on a careful design of the heterogeneous photocatalyst.

From this point of view, we propose herein the synthesis of two novel heterogeneous photocatalysts that incorporate **RB** covalently attached to the surface of silica nanoparticles with and without a core of magnetite. The new photocatalysts will be extensively characterized and tested together with homogeneous **RB** in the photodegradation of diclofenac (DCF), acetaminophen (ACF), and ofloxacin (OFX). In this context, a deep investigation on the operating mechanisms of the heterogeneous **RB** photocatalysts will be carried out on the basis of photophysical and photochemical experiments, taking into account the percentage of surface of silica nanoparticles covered by **RB,** as well as, the magnetic field produced by the magnetite core. Additionally, inactivation of Gram-positive and Gram-negative bacteria will be evaluated.

2. Materials and methods

2.1. Synthesis and characterization of supported photocatalysts

Synthesis **of SiO_2-RB** or **Fe_3O_4@SiO_2-RB** NPs and techniques for their characterization are described in SI.

2.2. Photodegradation experiments

Photodegradation of aqueous solutions of the pollutants at (5×10^{-5} M) were carried out in presence of 5×10^{-6} M (10% mol) **RB** in homogeneous media and in heterogeneous media with **SiO_2-RB** or **Fe_3O_4@SiO_2-RB** NPs, which, in the case of NPs corresponded to 0.8 mg mL^{-1} of **SiO_2-RB** and 0.44 mg mL^{-1} of **Fe_3O_4@SiO_2-RB**. Thus, samples were placed in 10 mL Pyrex glass tubes with magnetic stirring, and irradiated with LEDs at λ_{max} *ca* 527 nm under air and nitrogen atmospheres. More detail in Section 1 of SI.

2.3. Photodynamic antibacterial studies

Escherichia coli, *Pseudomonas aeruginosa,* and *Enterococcus faecalis* suspensions (4 mL, 1×10^6 CFU) were irradiated for 20 min in the presence of **SiO_2-RB** and **Fe_3O_4@SiO_2-RB** at two **RB** concentrations (2×10^{-5} M and 9×10^{-5} M). Periodically, aliquots (0.5 mL) of the bacterial suspensions were withdrawn, serially diluted in PBS, spread plated on PCA plates and incubated overnight to estimate the number of viable bacteria. More detail in Section 1 of SI.

2.4. Photophysical experiments

Fluorescence and singlet oxygen measurements as well as laser flash photolysis studies were performed with **SiO_2-RB** and **Fe_3O_4@SiO_2-RB** NPs using **RB** in homogeneous medium as reference to determine the behaviour of **RB** singlet and triplet excited state in heterogeneous media. Reactivity of contaminants with these intermediates and with $^1O_2$ was also evaluated. All details are described in Section 1 of SI.

3. Results and discussion

3.1. Synthesis of SiO_2-RB and Fe_3O_4@SiO_2-RB NPs

The two new heterogeneous photocatalysts (**SiO_2-RB** and **Fe_3O_4@-SiO_2-RB** NPs) were synthesized in several steps as shown in Scheme S1. Among the described methods for the synthesis of silica NPs, the microemulsion protocol was selected (see details in SI) since it could be applied for the preparation of the photocatalyst that incorporates a magnetite core (**Fe_3O_4@SiO_2-RB**). Briefly, a microemulsion of IGEPAL CO-520 in cyclohexane (in the absence or in the presence of previously synthesized Fe_3O_4 NPs) was treated with aqueous ammonia, which enters the Igepal CO-520 micelles, increases their size and forms the reverse microemulsion. Then, the added TEOS undergoes hydrolysis at the oil/water interface and finally condenses to form the silica shell. The resulting **SiO_2** or **Fe_3O_4@SiO_2** NPs were derivatized with APTES to give rise to a monolayer of free amino groups that fulfils two different goals: i) protects the silica from the aqueous media, and ii) facilitates the subsequent covalent bonding of **RB**. Thus, treatment of the **SiO_2-NH_2** / **Fe_3O_4@SiO_2-NH_2** NPs with **RB** under typical amide formation protocol, in the presence of EDC as the coupling agent, resulted into the formation of **SiO_2-RB** and **Fe_3O_4@SiO_2-RB** as pink powders, in which the strong covalent bond between the NPs and the chromophore prevents subsequent leaching of the dye into the homogeneous media. According to the pink color intensity, the presence of the magnetite core produced a higher **RB** loading (see Fig. S1A-B). In an attempt to maximize the number of **RB** moieties on the surface of the NPs, different concentrations of **RB** were employed, however, the same loading of **RB** resulted in the three cases (see Fig. S1C). Previous reports incorporated *ca.* two

orders of magnitude less **RB** on NPs of similar sizes [30]. Thus, the results obtained herein indicate that the specific arrangement of the chromophores on the surface may prevent higher loading.

3.2. Characterization of SiO_2-RB or Fe_3O_4@SiO_2-RB NPs

TEM (Fig. 1) and HRFSEM (Fig. S2) images corresponding to **SiO_2-RB** and **Fe_3O_4@SiO_2-RB** NPs (A and B, respectively) revealed that both synthetized NPs have a spherical morphology, identical to the NPs prior to derivatization (results not shown). The diameter size in both cases was similar (*ca.* 83.0 ± 0.6 nm for **SiO_2-RB**, and *ca.* 86 ± 5 nm for **Fe_3O_4@SiO_2-RB**) showing a homogeneous dispersion. In the case of the magnetic ones, the core has a diameter of *ca.* 18.0 ± 1.3 nm and most of the spheres contained the magnetite core. X-ray diffraction before and after anchoring **RB** confirmed the presence of SiO_2 together with the characteristic peaks corresponding to Fe_3O_4 in the case of **Fe_3O_4@SiO_2** (see Fig. S3) [32]. ^{29}Si solid NMR (Fig. 3C) shows the peaks characteristic of silica at − 97.91, − 107.50 and − 116.34 ppm, corresponding to $(SiO)_2Si(OH)_2$ (Q_2), $(SiO)_3SiOH$ (Q_3) and $(SiO)_4Si$ (Q_4), together with a peak at − 73.57, that could be safely assigned to the species

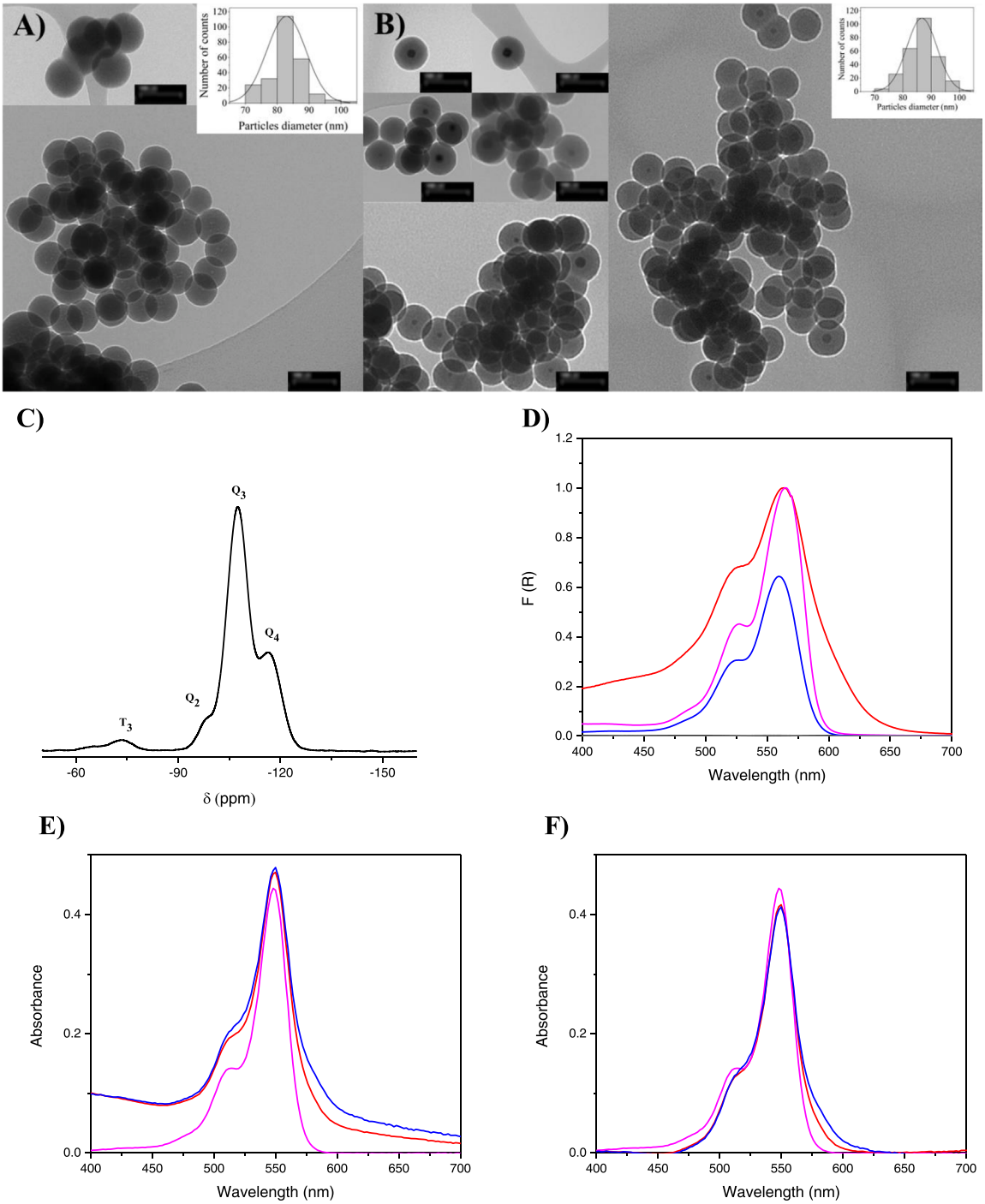

Fig. 1. TEM images for **SiO_2-RB** (**A**) and for **Fe_3O_4@SiO_2-RB** (**B**) and their size distribution (insets). **C)** ^{29}Si solid-state NMR spectra of **SiO_2-RB**; **D)** Diffuse reflectance spectra with baseline correction of **SiO_2 (gray)**, **SiO_2-RB** (**blue**), **Fe_3O_4@ -SiO_2-RB** (**red**) and **RB** (**pink**). Visible spectra of aqueous suspensions of **SiO_2-RB** (**blue**, 0.80 mg mL^{-1}), **Fe_3O_4@ -SiO_2-RB** NPs (**red,** 0.44 mg mL^{-1}) and **RB** (**pink**, 5 ×10^{-6} **M**) before baseline correction (**E**) and after baseline correction (**F**).

$(SiO)_3SiRNH$ (T_3), proving that the functionalization of NPs surface with APTES was successfully achieved [33]. Moreover, diffuse reflectance spectra showed the band with a shoulder, characteristic of **RB** with maxima at 563 nm and 559 nm for **SiO_2-RB** and **Fe_3O_4@SiO_2-RB** NPs, respectively, slightly blue-shifted compared to the solid pristine **RB** peaking at 564 nm (Fig. 3D). The amount of **RB** covalently linked to the surface of the **SiO_2-RB** and **Fe_3O_4@SiO_2** NPs was determined using two different methods: UV–vis spectroscopy and Inductively Coupled Plasma Mass Spectrometry (ICP-MS). For the first case, different aqueous suspensions of **SiO_2-RB** and **Fe_3O_4@SiO_2** NPs were prepared and the visible spectra were recorded before and after the baseline correction due to the light scattering associated to the NPs. The absorbance at the maximum was compared to a calibration curve of homogeneous **RB** (see Figs. 3E and 3F). By comparison of the given absorbances, a loading of **RB** of 0.63% (w/w) and 1.16% (w/w) was determined for **SiO_2-RB** and **Fe_3O_4@SiO_2-RB**, respectively. From these values, the portion of NPs surface covered by **RB** molecules was also estimated and corresponded to *ca.* 1/8 for **SiO_2-RB** NPs and *ca.* 1/4 for **Fe_3O_4@SiO_2-RB** NPs (procedure details are in SI). In addition, the **RB** loading on NPs was also determined from ICP-MS, based on the amount of iodine after microwave digestion. Results showed values of 8.76 ± 0.08 mg I/g and 10.57 ± 0.7 mg I/g for **SiO_2-RB** and **Fe_3O_4@SiO_2-RB** NPs, respectively. From these data, the determined **RB** loading was 1.6% and 2% (w/w) for **SiO_2-RB** and **Fe_3O_4@SiO_2-RB** NPs, respectively, in good agreement with the results obtained from the visible absorbance upon correction due to the light scattering. The fact that the portion of NPs surface covered by **RB** molecules was not increased adding more **RB** could be attributed to Coulombic repulsion between **RB** chromophores due to their anionic character. An alteration of this effect by the magnetic field produced by the magnetite core could also explain the higher **RB** loading of in the case of **Fe_3O_4@SiO_2-RB** NPs compared to **SiO_2-RB**. Based on the coverage of the particle surface in both materials, it could be anticipated that aggregation of chomophores will be prevented, and photophysical behaviour of **RB** will be similar to that of the known homogeneous **RB**. On the contrary, when riboflavin was covalently attached to the silica surface of microspheres producing a complete shell, the photophysical properties of riboflavin changed tremendously [26]. This case acts as a further example of the need of characterizing the photophysical properties of every new heterogenous photocatalyst instead of assuming those of the homogeneous one.

3.3. *Photodegradation of pollutants*

The results of the photodegradation experiments carried out in the presence of **SiO_2-RB** and **Fe_3O_4@SiO_2-RB** NPs, as well as the control irradiations under **RB** homogeneous conditions, under different atmospheres, are summarized in Fig. 2 (see Fig. S5 for the irradiation set-up). As it can be seen in the case of the heterogeneous irradiations, the magnetic core did not produce any significant effect on the photodegradations, and initial stirring in darkness resulted in *ca.* 10% decrease in the concentration of the drugs, due to a partial adsorption on the surface of the photocatalysts. Interestingly, heterogeneous irradiations resulted in higher photodegradation yields. More specifically, DCF was completely removed upon three hours of heterogeneous irradiation,

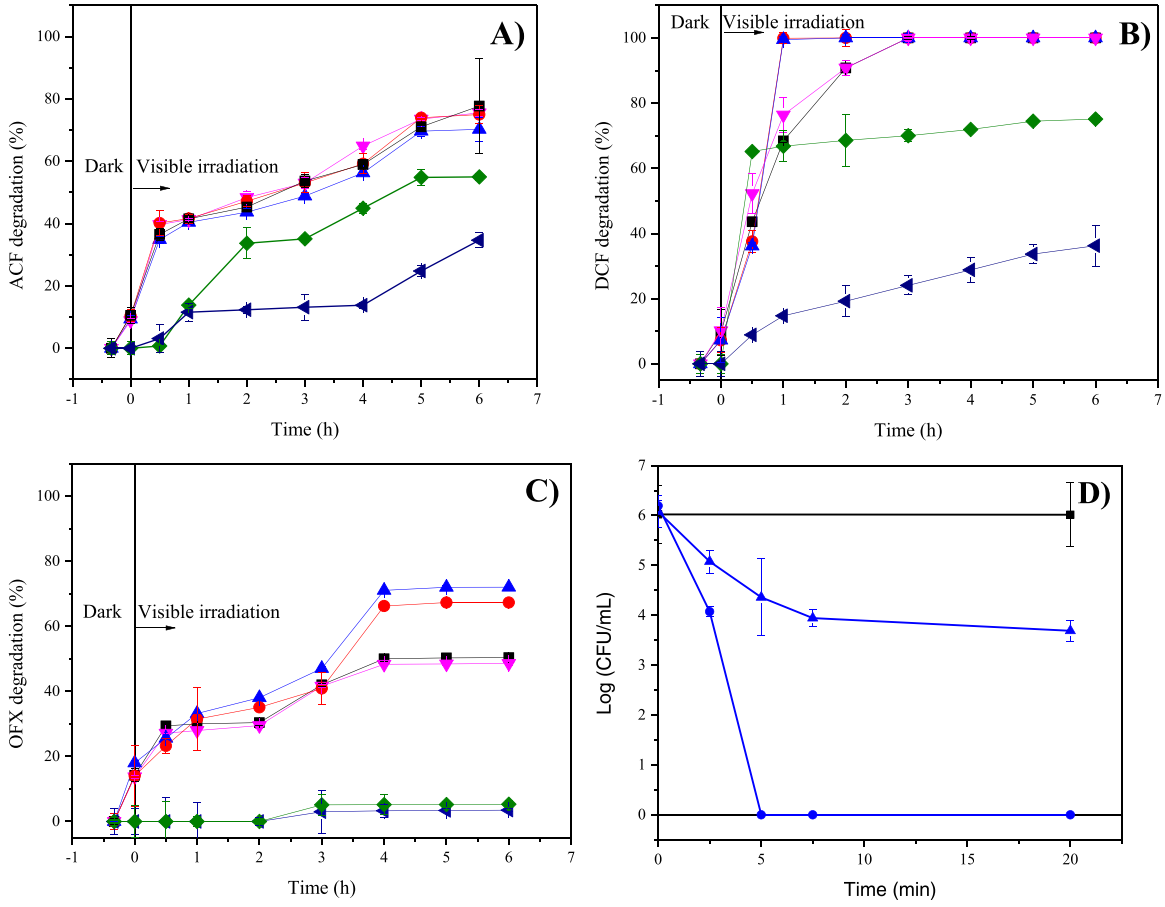

Fig. 2. Evaluation of the removal of ACF (**A**), DCF (**B**) and OFX (**C**) $C_0 = 5 \times 10^{-5}$ M each, *vs* irradiation time in the presence of **SiO_2-RB**_Air (●), **SiO_2-RB**_N_2 (■), **Fe_3O_4@SiO_2-RB**_Air (▲), **Fe_3O_4@SiO_2-RB**_N_2(▼), **RB**-homogeneous_Air (◀) and **RB**-homogeneous_N_2 (♦). [**RB**] = 5×10^{-6} M in aqueous suspensions/solutions. D) Survival curves of *E. faecalis* in the presence of **SiO_2-RB** at **RB** concentrations of 2×10^{-5} M (circles) and 9×10^{-5} M (triangles) after being irradiated with LED lamps (λ_{max} = 520 nm, 67.45 W m^{-2}). Control experiments were performed in the dark (■). Data are shown as mean ± standard deviation (n = 4). Results for *E. coli* and *P. aeruginosa* were identical to those observed in the dark (not shown).

up to 77% of removal of ACF was achieved upon 6 h irradiation, and 70% removal was observed after 4 h irradiation in the case of OFX. Nevertheless, the observed degradation under heterogeneous conditions can be considered very good, and in high contrast with the values observed under homogeneous conditions (around 30% for aerated homogeneous conditions in the case of DCF and ACF, and <5% for OFX). Association between OFX and the photocatalysts may be the reason of that enhancement (*vide infra*). Moreover, the removal of the drugs was mostly independent from the presence of air, pointing to a mechanism different from the participation of $^1O_2$. It is worth to mention that a higher photostability of **RB** upon heterogenization was observed in all the irradiations performed with the contaminants (see results using DCF in Fig. 3). Thereby, the reactivity of **RB** heterogeneous photocatalysts within the first hour of irradiation is maximum, independent from the drug, and it considerably drops as long as the drug concentration decreases.

3.4. Photodynamic inactivation of gram-negative and gram-positive bacteria

Photoinactivation experiments for *E. faecalis, E. coli* and *P. aeruginosa* were carried out in the presence of **SiO_2-RB** (Fig. 1D) and **Fe_3O_4@SiO_2-RB** NPs (Fig. S6). In order to obtain high efficiency in short times, two high photocatalyst concentrations (equivalent to [**RB**] = 2×10^{-5} M and 9×10^{-5} M), under irradiation at 520 nm, were evaluated. Both photocatalysts were highly efficient in inactivating the Gram-positive bacteria, *E. faecalis*, and both showed very similar photodynamic. In fact, *E. faecalis* survival curves for the low **RB** concentration (2×10^{-5}M) were practically identical for the two photocatalysts. Only 2.5 min after exposure to the green light, a reduction of viable colonies of more than 2 $\log_{10}$ units (bacterial inactivation >99%) was obtained, and 2.5 min later, the total bacterial inhibition was achieved in both cases. Interestingly, at the higher concentration (9×10^{-5}M), lower bacterial inactivation levels of 99.59% (2.3 $\log_{10}$ units) and 99.69% (2.9 $\log_{10}$ units) were obtained for **SiO_2-RB** and **Fe_3O_4@SiO_2-RB** NP, respectively, after 20 min of irradiation. The lower antibacterial efficiency found at higher

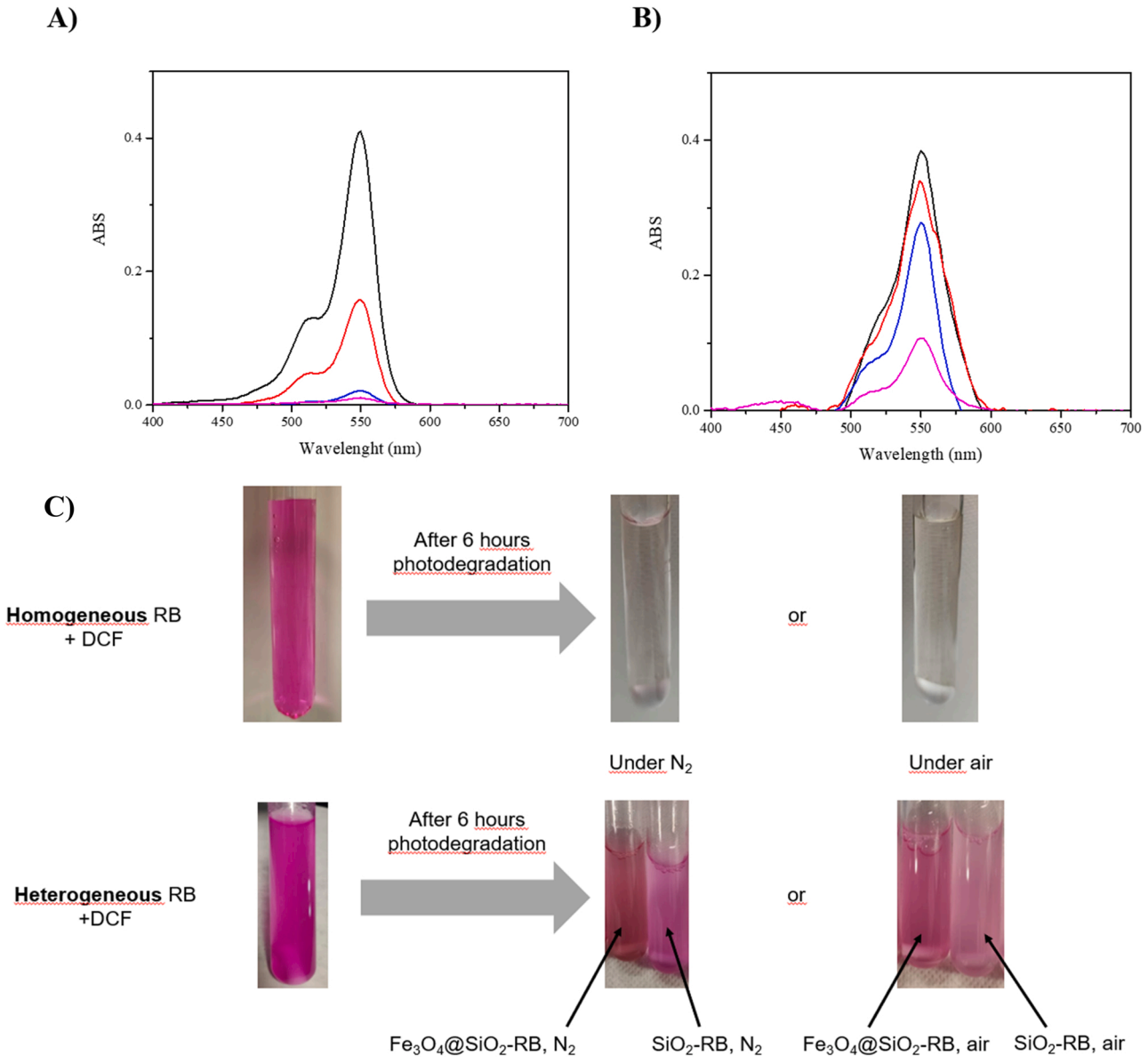

Fig. 3. Visible spectra of homogeneous-**RB** (**A**) and suspension-**Fe_3O_4@-SiO_2-RB** (**B**) (with baseline correction) with DCF under air (10 mL, 5×10^{-6} M in water) at different irradiation times: **0 h** (**black**), **1 h** (**red**), **3 h** (**blue**) and **6 h (pink)** and (**C**) real pictures showing changes in the pink color upon irradiation.

concentration of **RB** could be attributed to the formation of aggregates that negatively affect singlet oxygen generation [29,34]. For comparative purposes, *E. faecalis* was also exposed to a homogeneous solution of **RB** (2×10^{-5} M). Similarly, bacterial inhibition was fully complete 5 min after exposure to the light, while in dark conditions, no reduction of viable counts was obtained after 20 min (results not shown). These similar results showed by the two NPs and free **RB** clearly prove that the antimicrobial photodynamic activity of **RB** is not altered when this photosensitizer is covalently linked to silica NPs.

Our results against Gram-positive bacteria showed that using higher concentrations of **RB** than those usually reported for disinfection purposes was an acceptable strategy as it improved the efficiency [29,30]. According to Guo et al. [30], **RB**-decorated silica nanoparticles evaluated at a concentration equivalent to [**RB**] of 3 μM and with an illumination intensity of light source (525 nm) of approx. 33 J/cm^2, is able to reach a seven-order-of magnitude reduction in the viability count after 40 min of exposure. However, in our case, a quantity of nanoparticles corresponding to a [**RB**] of 20 μM and with a lesser illumination intensity of light source (520 nm) of 8.1 J/cm^2, the time required for fully complete bacterial inactivation was only 5 min. In this case, the initial bacterial concentration evaluated was 1×10^6 ufc/mL, which is a bacterial concentration usually found in sewage. Nevertheless, the use of high photocatalyst concentrations should be optimized in order to avoid the formation of aggregates than negatively affects the photodynamic activity, as has been shown to happen regarding the highest concentration assayed in this work.

On the other hand, no inhibition was observed for *E. coli* and *P. aeruginosa*, at any of the concentrations tested, neither in the presence of the heterogeneous photocatalysts nor homogeneous **RB**, despite the relatively high concentrations of **RB** or the increase of irradiation time up to 1 h. It has been widely reported that Gram-negative bacteria are more resistant to photodynamic bactericidal activity than Gram-positive bacteria due to their highly organized outer wall [35]. Moreover, electrostatic repulsion forces between the anionic **RB** and the highly negatively charged outer layer of the Gram-negative bacteria could prevent the interaction **RB**-bacterium and consequently the effect of **RB** photodynamic activity. In this sense, surface modification of the synthesized NPs by introducing positive charges could improve their disinfection activity as the nanoparticles would become active against Gram-negative bacteria. This effect has been recently proven in a **RB**-glass wool-based photocatalyst [36].

3.5. Photophysical results

3.5.1. Singlet excited state of RB in SiO_2-RB and Fe_3O_4@SiO_2-RB NPs

Properties of **RB** singlet excited state (^{1}**RB***) in the photocatalysts **SiO$_2$-^{1}RB*** and **Fe$_3$O$_4$@SiO$_2$-^{1}RB*** were investigated registering their fluorescence emission spectra in aqueous suspensions and comparing the results to a homogeneous solution of **RB** at the same absorbance at the excitation wavelength (see Fig. S7). The emission maxima (at *ca.* 567 nm), as well as the emission intensity observed for the three materials were pretty much identical. Thus, **RB** fluorescence quantum yield (Φ_F) in the NPs will be approximately the same as that described for **RB** in homogeneous solutions ($\Phi_F = 0.018$) [17]. Emission lifetimes of **RB** in the heterogeneous photocatalysts could not be determined since they were below the detection limit of our equipment. This fact agrees with a ^{1}**RB*** lifetime for **SiO$_2$-RB** and **Fe$_3$O$_4$@SiO$_2$-RB** similar to that described in the literature for **RB** in homogeneous aqueous solution (τ_F <0.1 ns) [37]. Thereby, we could anticipate that reactivity of ^{1}**RB*** would be the same in bulk aqueous media than when it is covalently linked to the silica of NPs, with and without the presence of a magnetite core. This hypothesis was confirmed by quenching of the steady-state emission upon increasing amounts of ACF and DCF (see Fig. S8 for the results of ACF and DCF in **SiO$_2$-RB** and **Fe$_3$O$_4$@SiO$_2$-RB** NPs and Fig. S9 for the homogeneous **RB**). For the case of OFX, the static quenching was determined from the decrease in the bleaching of **RB** at the initial time after laser excitation, from LFP experiments (Fig. S10). The static quenching constants (K) determined from these experiments are shown in Table S1. They revealed a behaviour of ^{1}**RB*** with ACF, DCF and OFX in the bulk aqueous media very similar to that showed when ^{1}**RB*** was generated in **SiO$_2$-RB** and **Fe$_3$O$_4$@SiO$_2$-RB** NPs.

In parallel, thermodynamic calculations were made to evaluate the feasibility of the electron transfer from the drugs to the excited states of **RB** using the reported E_{red} values: E_{red} (RB/RB$^{\cdot-}$) = −0.78 V [38], E_{red} (ACF$^{\cdot+}$/ACF) = +1.15 V [20], E_{red} (DCF$^{\cdot+}$/DCF) = +0.75 V [20], E_{red} (OFX$^{\cdot+}$/OFX) = +1.21 V [39], all *vs* SCE, and the energies of the ^{1}**RB*** and ^{3}**RB*** (2.17 and 1.80 eV, respectively [20,37], see Section 7 in the SI). The calculated ΔG values indicated that the processes were exergonic in all cases to the ^{1}**RB*** and should be diffusion controlled. Thus, assuming diffusion rate constant at room temperature of *ca.* 7.4×10^9 M^{-1} s^{-1} [40] and the τ_F of ^{1}**RB*** is *ca.* 0.1 ns in water [37], the Stern Volmer constant ($K_{sv} = k_q$ x τ_F) for these reactions would be *ca.* 0.3 M^{-1}. Upon comparing the K_{SV} to the obtained K values (see Table S1), we could safely discard a relevant influence of dynamic processes in the observed **RB** fluorescence quenching for ACF, DCF and OFX. Thus, the observed static quenching constants mainly correspond to association constants (K_a). In the particular case of OFX, the K_a value under homogeneous conditions is higher than that for ACF and DCF; even more, in the presence of **SiO$_2$-RB** and **Fe$_3$O$_4$@SiO$_2$-RB NPs** it increases 4- and 9-fold, respectively. This increase is in parallel with the higher photodegradation yield for this drug under heterogeneous *versus* homogeneous conditions (*vide supra*).

3.5.2. Triplet excited state of RB in SiO_2-RB and Fe_3O_4@SiO_2-RB NPs

Laser flash photolysis studies were performed with **RB** in homogeneous aqueous solution and in suspensions of **SiO$_2$-RB** and **Fe$_3$O$_4$@SiO$_2$-RB** NPs. **RB** triplet excited state (^{3}**RB***) detected in the three systems showed identical transient absorption spectrum, with bands at λ_{max} *ca.* 370, 470 and 600 nm, and an intense bleaching centred at 560 nm due to the depopulation of **RB** ground state, which fully agree with the literature (Fig. S11A) [37]. Moreover, no differences in signal intensity or ^{3}**RB*** lifetime (τ_T *ca.* 63 μs) were observed between homogeneous and heterogeneous systems (see inset Fig. S11A). These results are in accordance to the percentage of surface area covered by **RB** on the shell of **SiO$_2$-RB** and **Fe$_3$O$_4$@SiO$_2$-RB** NPs determined by UV-Vis spectroscopy (*ca* 1/8 and 1/4 respectively of the total surface of NPs), where any interaction between an excited **RB** state and a **RB** in the ground state is almost impossible. Thus, as photophysical properties of ^{1}**RB*** and ^{3}**RB*** were not modified upon covalent attachment of **RB** to NPs with and without a magnetite core, the **RB** intersystem crossing quantum yield (Φ_{ISC}) in the NPs would be approximately the same as that described for **RB** in homogeneous solutions (Φ_{ISC} = 0.8–0.98) [29, 41]. Therefore, the transient absorption spectra upon addition of the drugs were obtained from aqueous solutions of **RB** (Fig. S12B-D). No new signals were observed except from an aniline radical derivative generated from the DCF electron transfer reaction [42]. Considering these results, and that reactivity of ^{1}**RB*** also resulted to be similar in the three systems, bimolecular rate constants between ^{3}**RB*** and ACF, DCF and OFX (k_{qT}) were only determined in the homogeneous medium (see Fig. S13). The determined values (see Table S2) are in good agreement with the estimated ΔG values (see Section 7 of SI), since other factors like back electron transfer or separation of the radical ion pair after quenching are not considered [43]. Interestingly, the k_{qT} values obtained for the three drugs resulted to be 10 times higher than those described in the literature [15]. However, our data have been determined in aqueous media and the other ones were obtained using acetonitrile as a solvent and it is well known that polar solvents such as water favour Type I mechanisms due to their higher capability to stabilize charged species. Thereby, this finding reveals that to analyse all the kinetics in photosensitized reactions, the k_{qT} must be determined using the solvent of the reaction medium, especially when this solvent is water.

3.5.3. Generation and reactivity of $^1O_2$

The generation of singlet oxygen was also registered in homogeneous solution of **RB** and in suspensions of **SiO_2-RB** and **Fe_3O_4@SiO_2-RB** NPs using D_2O as solvent. Even in this case, no differences in signal intensity or lifetime of $^1O_2$ were observed between homogeneous and heterogeneous systems as displayed in Fig. S14. For this reason, bimolecular rate constants between $^1O_2$ and ACF, DCF and OFX (k_{q1O2}) were only determined in the homogeneous phase (see Fig. S15), the obtained bimolecular rate constants are shown in Table S2. Values in the order of 10^{-6} $M^{-1}s^{-1}$ were found in the literature for fluoroquinolones in neutral phosphate buffer using the same methodology [44]. In our experiments, **RB** was replaced by perinaphthenone (PN) as singlet oxygen generator due to its higher $^1O_2$ formation yield [45].

3.5.4. Kinetic analysis

All the determined quenching rate constants of the singlet and triplet excited states of the **RB** and the two heterogeneous photocatalysts, the quenching of singlet oxygen, together with the employed concentration of the drugs and the photophysical parameters of **RB** were combined to evaluate the contribution of each potential deactivation pathway, based on the equations reported in the Section 10 of the SI. The calculated contribution of each quenching processes is shown in Table S3. As it could be anticipated from the lifetime of singlet excited state of **RB**, the contribution of quenching of ^{1}**RB*** is negligible, unless there is a pre-association. In fact, association between **RB** and the drugs results in complexes that eventually reach the singlet excited state and can result into oxidation of the drugs by electron transfer. The contribution of this pathway depends on the value of the association constant, and thus is the most important one in the case of OFX. Nevertheless, in previous reports on riboflavin with low association constants to pollutants, the formation of complexes was the only responsible species for the overall photodegradation [26]; thus, their contribution in the case of ACF and DCF should not be disregarded. Finally, under the employed concentration of the drugs (5×10^{-5} M) and considering that the lifetime of $^1O_2$ in water is *ca.* 3.5 μs [46], the contribution to the Type II mechanism results negligible.

Even more, the oxidation of the bacteria membranes must be mainly produced by reaction with the $^1O_2$ generated from ^{3}**RB*** [47]. Nevertheless, the observed inactivation of bacteria could also be explained based on the expected association of the bacteria on the heterogeneous **SiO_2-RB** and **Fe_3O_4@ -SiO_2-RB** NPs. Upon association, electron transfer processes could happen to the excited ^{1}**RB*** , as previously demonstrated using cell-wall compounds of bacteria [48].

In the case of photodegradation of drugs, this mainly happens through electron transfer to the ^{3}**RB*** and to the short-lived ^{1}**RB*** after adsorption as shown in Scheme 1. Moreover, the reuse of heterogeneous **SiO_2-RB** and **Fe_3O_4@ -SiO_2-RB** NPs will be optimum after 1 h irradiation under the evaluated conditions. Afterwards, the speed in the photodegradation of the drugs starts to drop, associated to the decrease in the concentration of the electron donor pollutant, and consequently higher $^1O_2$ production. Eventually, the $^1O_2$ will produce the oxidation of **RB**, but after 1 h its degradation is still insignificant (see Fig. 3B).

4. Conclusions

New heterogeneous nanosized photocatalysts incorporating Rose Bengal (**RB**) have been prepared. They were based on the covalent anchoring of the chromophore to the surface of SiO_2 nanoparticles, and SiO_2 nanoparticles incorporating a magnetite core, respectively. They have demonstrated to efficiently achieve photodegradation of ACF, DCF, and OFX under visible-light irradiation, with greater efficiency in the case of DCF. Interestingly, the photophysical properties of **RB** remain unchanged, although the photostability of **RB** anchored to the heterogeneous materials is higher than in homogeneous media. The presence of magnetite core in the heterogeneous photocatalyst facilitates its recovery from the medium and increased the **RB** loading to the shell, without modifying the photophysical properties of the heterogeneous **RB** photocatalyst. These new photocatalysts also show a great efficiency in the photoinactivation of Gram-positive bacteria. Analysis of all constants involving the photosensitized degradations of ACF, DCF, and OFX has evidenced that electron transfer processes between **RB**, in homogeneous solutions and as a heterogeneous photocatalyst, and the three drugs are the initial step of their oxidations. Moreover, in the case of OFX initial association to **RB** plays a significant role.

CRediT authorship contribution statement

J. Flores: experimental work and treatment of data; P. Moya: design of microbiological work and treatment and discussion of data; F. Bosca: design of the Project, discussion of results and writting and revising the MS; M.L. Marin: design of the Project, discussion of results and writting and revising the MS.

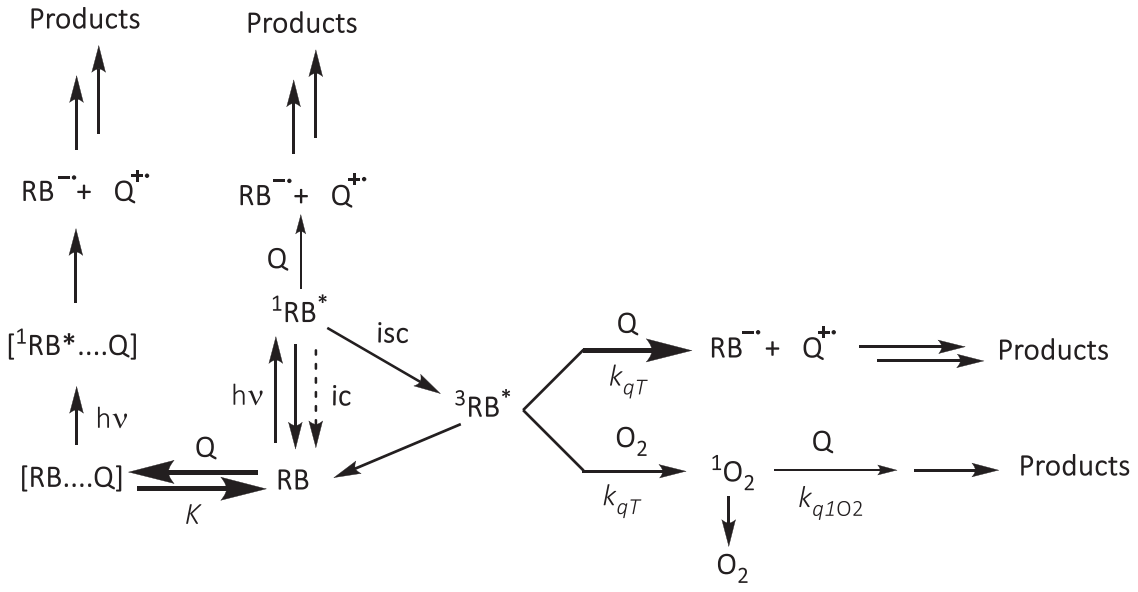

Scheme 1. Overall postulated mechanistic pathway operating in the photodegradation of ACF, DCF and OFX by **RB**, **SiO_2-RB** and **Fe_3O_4@ -SiO_2-RB** NPs.

Declaration of Competing Interest

The authors declare that they have no known competing financial interests or personal relationships that could have appeared to influence the work reported in this paper.

Data Availability

Data will be made available on request.

Acknowledgments

PhD Scholarship from CONACYT for Flores-Garcia J. (709358), and the Spanish Ministry of Science and Innovation (PID2019-110441RB-C33 financed by MCIN/AEI/10.13039/501100011033) are gratefully acknowledged.

Appendix A. Supporting information

Supplementary data associated with this article can be found in the online version at doi:10.1016/j.cattod.2023.01.001.

References

[1] M.M. Bello, A.A.A. Raman, Adsorption and Oxidation Techniques to Remove Organic Pollutants from Water, in: 2018: pp. 249–300. https://doi.org/10.1007/978–3-319–92111-2_8.
[2] Y. Mameri, N. Debbache, M. el mehdi, N. Benacherine, T. Seraghni, Sehili, Heterogeneous photodegradation of paracetamol using Goethite/H 2 O 2 and Goethite/oxalic acid systems under artificial and natural light, J. Photochem. Photobio. A Chem. 315 (2016) 129–137, https://doi.org/10.1016/j.jphotochem.2015.09.019.
[3] Adeniji Ohoro, Okoh Okoh, Distribution and chemical analysis of pharmaceuticals and personal care products (PPCPs) in the environmental systems: a review, Int J. Environ. Res Public Health 16 (2019) 3026, https://doi.org/10.3390/ijerph16173026.
[4] Y. Valcárcel, S.G. Alonso, J.L. Rodríguez-Gil, R.R. Maroto, A. Gil, M. Catalá, Analysis of the presence of cardiovascular and analgesic/anti-inflammatory/antipyretic pharmaceuticals in river- and drinking-water of the Madrid Region in Spain, Chemosphere 82 (2011) 1062–1071, https://doi.org/10.1016/j.chemosphere.2010.10.041.
[5] A. Nasiri, F. Tamaddon, M.H. Mosslemin, M. Amiri Gharaghani, A. Asadipour, Magnetic nano-biocomposite CuFe2 O4 @methylcellulose (MC) prepared as a new nano-photocatalyst for degradation of ciprofloxacin from aqueous solution, Environ. Health Eng. Manag. 6 (2019) 41–51, https://doi.org/10.15171/EHEM.2019.05.
[6] X. Ren, Y. Zhang, L. Yang, Z. Chen, Degradation of ofloxacin by peroxymonosulfate activated with cobalt-doped graphitic carbon nitride: mechanism and performance, Inorg. Chem. Commun. 133 (2021), 108863, https://doi.org/10.1016/j.inoche.2021.108863.
[7] J. Radjenović, M. Petrović, D. Barceló, Fate and distribution of pharmaceuticals in wastewater and sewage sludge of the conventional activated sludge (CAS) and advanced membrane bioreactor (MBR) treatment, Water Res. 43 (2009) 831–841, https://doi.org/10.1016/j.watres.2008.11.043.
[8] G. Maniakova, M.I. Polo-López, I. Oller, M.J. Abeledo-Lameiro, S. Malato, L. Rizzo, Simultaneous disinfection and microcontaminants elimination of urban wastewater secondary effluent by solar advanced oxidation sequential treatment at pilot scale, J. Hazard. Mater. 436 (2022), 129134, https://doi.org/10.1016/j.jhazmat.2022.129134.
[9] P. Fernández-Castro, M. Vallejo, M.F. San Román, I. Ortiz, Insight on the fundamentals of advanced oxidation processes. Role and review of the determination methods of reactive oxygen species, J. Chem. Technol. Biotechnol. 90 (2015) 796–820, https://doi.org/10.1002/jctb.4634.
[10] M.R. Hoffmann, S.T. Martin, W. Choi, D.W. Bahnemann, Environmental applications of semiconductor photocatalysis, Chem. Rev. 95 (1995) 69–96, https://doi.org/10.1021/cr00033a004.
[11] A.R. Ribeiro, O.C. Nunes, M.F.R. Pereira, A.M.T. Silva, An overview on the advanced oxidation processes applied for the treatment of water pollutants defined in the recently launched Directive 2013/39/EU, Environ. Int 75 (2015) 33–51, https://doi.org/10.1016/j.envint.2014.10.027.
[12] S. Giannakis, S. Rtimi, C. Pulgarin, Light-assisted advanced oxidation processes for the elimination of chemical and microbiological pollution of wastewaters in developed and developing countries, Molecules 22 (2017) 1070, https://doi.org/10.3390/molecules22071070.
[13] A. Kumar, P. Raizada, P. Singh, R. v Saini, A.K. Saini, A. Hosseini-Bandegharaei, Perspective and status of polymeric graphitic carbon nitride based Z-scheme photocatalytic systems for sustainable photocatalytic water purification, Chem. Eng. J. 391 (2020), 123496, https://doi.org/10.1016/j.cej.2019.123496.
[14] P. Raizada, A. Sudhaik, P. Singh, P. Shandilya, A.K. Saini, V.K. Gupta, J.-H. Lim, H. Jung, A. Hosseini-Bandegharaei, Fabrication of Ag3VO4 decorated phosphorus and sulphur co-doped graphitic carbon nitride as a high-dispersed photocatalyst for phenol mineralization and E. coli disinfection, Sep Purif. Technol. 212 (2019) 887–900, https://doi.org/10.1016/j.seppur.2018.12.007.
[15] P. Singh, A. Sudhaik, P. Raizada, P. Shandilya, R. Sharma, A. Hosseini-Bandegharaei, Photocatalytic performance and quick recovery of BiOI/Fe3O4@graphene oxide ternary photocatalyst for photodegradation of 2,4-dintirophenol under visible light, Mater. Today Chem. 12 (2019) 85–95, https://doi.org/10.1016/j.mtchem.2018.12.006.
[16] V. Hasija, A. Sudhaik, P. Raizada, A. Hosseini-Bandegharaei, P. Singh, Carbon quantum dots supported AgI /ZnO/phosphorus doped graphitic carbon nitride as Z-scheme photocatalyst for efficient photodegradation of 2, 4-dinitrophenol, J. Environ. Chem. Eng. 7 (2019), 103272, https://doi.org/10.1016/j.jece.2019.103272.
[17] M.L. Marin, L. Santos-Juanes, A. Arques, A.M. Amat, M.A. Miranda, Organic photocatalysts for the oxidation of pollutants and model compounds, Chem. Rev. 112 (2012) 1710–1750, https://doi.org/10.1021/cr2000543.
[18] R. Martinez-Haya, J. Gomis, A. Arques, A.M. Amat, M.A. Miranda, M.L. Marin, Direct detection of the triphenylpyrylium-derived short-lived intermediates in the photocatalyzed degradation of acetaminophen, acetamiprid, caffeine and carbamazepine, J. Hazard Mater. 356 (2018) 91–97, https://doi.org/10.1016/j.jhazmat.2018.05.023.
[19] C. Spagnul, L.C. Turner, R.W. Boyle, Immobilized photosensitizers for antimicrobial applications, J. Photochem. Photobio. B 150 (2015) 11–30, https://doi.org/10.1016/j.jphotobiol.2015.04.021.
[20] R. Martinez-Haya, M.A. Miranda, M.L. Marin, Type I vs Type II photodegradation of pollutants, Catal. Today 313 (2018) 161–166, https://doi.org/10.1016/j.cattod.2017.10.034.
[21] J.A. Rengifo-Herrera, J. Sanabria, F. Machuca, C.F. Dierolf, C. Pulgarin, G. Orellana, A comparison of solar photocatalytic inactivation of waterborne E. coli Using Tris (2,2′-bipyridine)ruthenium(II), rose bengal, and TiO2, J. Sol. Energy Eng. 129 (2007) 135–140, https://doi.org/10.1115/1.2391319.
[22] E.A. Serna-Galvis, J.A. Troyon, S. Giannakis, R.A. Torres-Palma, C. Minero, D. Vione, C. Pulgarin, Photoinduced disinfection in sunlit natural waters: measurement of the second order inactivation rate constants between E. coli and photogenerated transient species, Water Res. 147 (2018) 242–253, https://doi.org/10.1016/j.watres.2018.10.011.
[23] S. Wang, Z. Zhang, B. Liu, J. Li, Silica coated magnetic Fe3O4 nanoparticles supported phosphotungstic acid: a novel environmentally friendly catalyst for the synthesis of 5-ethoxymethylfurfural from 5-hydroxymethylfurfural and fructose, Catal. Sci. Technol. 3 (2013) 2104, https://doi.org/10.1039/c3cy00223c.
[24] H.L. Ding, Y.X. Zhang, S. Wang, J.M. Xu, S.C. Xu, G.H. Li, Fe $_3$ O $_4$ @SiO $_2$ core/shell nanoparticles: the silica coating regulations with a single core for different core sizes and shell thicknesses, Chem. Mater. 24 (2012) 4572–4580, https://doi.org/10.1021/cm302828d.
[25] D. Palma, A. Bianco Prevot, M. Brigante, D. Fabbri, G. Magnacca, C. Richard, G. Mailhot, R. Nisticò, New insights on the photodegradation of caffeine in the presence of bio-based substances-magnetic iron oxide hybrid nanomaterials, Materials 11 (2018) 1084, https://doi.org/10.3390/ma11071084.
[26] O. Cabezuelo, R. Martinez-Haya, N. Montes, F. Bosca, M.L. Marin, Heterogeneous riboflavin-based photocatalyst for pollutant oxidation through electron transfer processes, Appl. Catal. B 298 (2021), 120497, https://doi.org/10.1016/j.apcatb.2021.120497.
[27] S. Demartis, A. Obinu, E. Gavini, P. Giunchedi, G. Rassu, Nanotechnology-based rose Bengal: a broad-spectrum biomedical tool, Dyes Pigments 188 (2021), 109236, https://doi.org/10.1016/j.dyepig.2021.109236.
[28] Y. Liu, X. Liu, Y. Xiao, F. Chen, F. Xiao, A multifunctional nanoplatform based on mesoporous silica nanoparticles for imaging-guided chemo/photodynamic synergetic therapy, RSC Adv. 7 (2017) 31133–31141, https://doi.org/10.1039/C7RA04549B.
[29] B. Martins Estevão, F. Cucinotta, N. Hioka, M. Cossi, M. Argeri, G. Paul, L. Marchese, E. Gianotti, Rose Bengal incorporated in mesostructured silica nanoparticles: structural characterization, theoretical modeling and singlet oxygen delivery, Phys. Chem. Chem. Phys. 17 (2015) 26804–26812, https://doi.org/10.1039/C5CP03564C.
[30] Y. Guo, S. Rogelj, P. Zhang, Rose Bengal-decorated silica nanoparticles as photosensitizers for inactivation of gram-positive bacteria, Nanotechnology 21 (2010), 065102, https://doi.org/10.1088/0957-4484/21/6/065102.
[31] N. Macia, R. Bresoli-Obach, S. Nonell, B. Heyne, Hybrid silver nanocubes for improved plasmon-enhanced singlet oxygen production and inactivation of bacteria, J. Am. Chem. Soc. 141 (2019) 684–692, https://doi.org/10.1021/jacs.8b12206.
[32] M. Khan, C.S.L. Fung, A. Kumar, I.M.C. Lo, Magnetically separable BiOBr/Fe3O4@SiO2 for visible-light-driven photocatalytic degradation of ibuprofen: mechanistic investigation and prototype development, J. Hazard Mater. 365 (2019) 733–743, https://doi.org/10.1016/j.jhazmat.2018.11.053.
[33] S.M. Soria-Castro, B. Lebeau, M. Cormier, S. Neunlist, T.J. Daou, J.P. Goddard, Organic/inorganic heterogeneous silica-based photoredox catalyst for aza-henry reactions, Eur. J. Org. Chem. 2020 (2020) 1572–1578, https://doi.org/10.1002/ejoc.201901382.
[34] H.B. Rodríguez, M.G. Lagorio, E.S. Román, Rose Bengal adsorbed on microgranular cellulose: evidence on fluorescent dimers, Photochem. Photobiol. Sci. 3 (2004) 674–680, https://doi.org/10.1039/B402484B.

[35] M.Q. Mesquita, C.J. Dias, M.P.M.S. Neves, A. Almeida, M.F. Faustino, Revisiting current photoactive materials for antimicrobial photodynamic therapy, Molecules 23 (2018) 2424, https://doi.org/10.3390/molecules23102424.
[36] A. Blázquez-Moraleja, P. Moya, M.L. Marin, F. Bosca, Synthesis of novel heterogeneous photocatalysts based on Rose Bengal for effective wastewater disinfection and decontamination, Catal. Today (2022), https://doi.org/10.1016/j.cattod.2022.11.009.
[37] L. Ludvíková, P. Friš, D. Heger, P. Šebej, J. Wirz, P. Klán, Photochemistry of rose bengal in water and acetonitrile: a comprehensive kinetic analysis, Phys. Chem. Chem. Phys. 18 (2016) 16266–16273, https://doi.org/10.1039/C6CP01710J.
[38] N.A. Romero, D.A. Nicewicz, Organic photoredox catalysis, Chem. Rev. 116 (2016) 10075–10166, https://doi.org/10.1021/acs.chemrev.6b00057.
[39] P. Talay Pinar, Electrochemical behaviour of ofloxacin in pharmaceutical and biological samples using a boron-doped diamond electrode in using anionic surfactant, Gazi Univ. J. Sci. 31 (2018).
[40] S.L. Murov, I. Carmichael, G.L. Hug. Handbook of Photochemistry, second ed., Marcel Dekker, New York, 2009.
[41] J. Park, K. An, Y. Hwang, J.-G. Park, H.-J. Noh, J.-Y. Kim, J.-H. Park, N.-M. Hwang, T. Hyeon, Ultra-large-scale syntheses of monodisperse nanocrystals, Nat. Mater. 3 (2004) 891–895, https://doi.org/10.1038/nmat1251.
[42] L. Qin, G.N.R. Tripathi, R.H. Schüler, Radiation chemical studies of the oxidation of aniline in aqueous solution, Z. Für Naturforsch. A 40 (1985) 1026–1039, https://doi.org/10.1515/zna-1985-1009.
[43] C.R. Lambert, I.E. Kochevar, Electron transfer quenching of the rose bengal triplet state, Photochem. Photobio. 66 (1997) 15–25, https://doi.org/10.1111/j.1751-1097.1997.tb03133.x.
[44] L.J. Martinez, R.H. Sik, C.F. Chignell, Fluoroquinolone antimicrobials: singlet oxygen, superoxide and phototoxicity, Photochem. Photobio. 67 (1998) 399–403, https://doi.org/10.1111/j.1751-1097.1998.tb05217.x.
[45] R. Schmidt, C. Tanielian, R. Dunsbach, C. Wolff, Phenalenone, a universal reference compound for the determination of quantum yields of singlet oxygen O2 (1Δg) sensitization, J. Photochem. Photobio. A Chem. 79 (1994) 11–17, https://doi.org/10.1016/1010-6030(93)03746-4.
[46] M. Bregnhøj, M. Westberg, F. Jensen, P.R. Ogilby, Solvent-dependent singlet oxygen lifetimes: temperature effects implicate tunneling and charge-transfer interactions, Phys. Chem. Chem. Phys. 18 (2016) 22946–22961, https://doi.org/10.1039/C6CP01635A.
[47] H.-S. Kim, E.J. Cha, H.-J. Kang, J.-H. Park, J. Lee, H.-D. Park, Antibacterial application of covalently immobilized photosensitizers on a surface, Environ. Res 172 (2019) 34–42, https://doi.org/10.1016/j.envres.2019.01.002.
[48] I. Berruti, M. Inmaculada Polo-López, I. Oller, J. Flores, M. Luisa Marin, F. Bosca, Sulfate radical anion: laser flash photolysis study and application in water disinfection and decontamination, Appl. Catal. B 315 (2022), 121519, https://doi.org/10.1016/j.apcatb.2022.121519.